Express Polymer Letters Vol.18, No.1 (2024) 72–87
Available online at www.expresspolymlett.com
https://doi.org/10.3144/expresspolymlett.2024.6

Research article

Effective nanoparticulate-type encapsulation delivery system for hydrophilic proteins and peptides

Flavio Massignan[1,2], *Gergő Gyulai*[1], *Kata Horváti*[3], *Szilvia Bősze*[4], *Éva Kiss*[1*]

[1]Laboratory of Interfaces and Nanostructures, Institute of Chemistry, Eötvös Loránd University, Pázmány Péter Sétány 1/A, H-1117 Budapest, Hungary
[2]Hevesy György Ph.D. School of Chemistry, Eötvös Loránd University, P.O. Box 32, H-1518 Budapest, Hungary
[3]MTA-TTK Lendület "Momentum" Peptide-Based Vaccines Research Group, Institute of Materials and Environmental Chemistry, Research Centre for Natural Sciences, Magyar Tudósok Körútja 2. H-1117 Budapest, Hungary
[4]Eötvös Loránd Kutatási Hálózat-Eötvös Loránd Tudományegyetem (ELKH-ELTE) Research Group of Peptide Chemistry, Eötvös Loránd Research Network, Eötvös Loránd University, Pázmány Péter sétány 1/A, H-1117 Budapest, Hungary

Received 24 August 2023; accepted in revised form 11 October 2023

Abstract. The elaboration of potent delivery systems for peptides/proteins is still a challenge but is increasingly needed in advanced therapy. In the present research, we have developed a nanoencapsulation system for peptides/proteins, which is suitable for the delivery of hydrophilic bioactive compounds. The preparation method combines the advantageous properties of reverse nanoemulsion and nanoprecipitation, resulting in the formation of nanoparticles in the size range of 350–500 nm. The polymeric coating composed of polycaprolactone allows chemical functionalization and protection while the inner microenvironment (containing 1-decanoyl-rac-glycerol and *N*,*N*-dimethyldodecylamine *N*-oxide surfactants) provides aqueous surrounding for the active with structural fidelity. Hen egg white lysozyme and β-lactoglobulin were successfully encapsulated, achieving protein contents of 10–60 μg/mg and encapsulation efficiencies ranging from 5–50% depending on the protein type and loading concentration. *In vitro* release measurement showed a biphasic sustained release profile of both proteins in the time range of one month. *In vitro* cytotoxicity investigation of protein-loaded nanoparticles exhibited good cell viability (above 95% at the highest treatment concentration of 0.3 mg/ml). The encapsulated membrane-active peptides have shown improved bioactivity.

Keywords: *drug delivery system, polymeric nanoparticles, proteins, cell-penetrating peptides, sustained release*

1. Introduction

Proteins and peptides are increasingly recognized as valuable therapeutic agents [1] as well as protein/peptide-based drug delivery systems [2]. They can function as hormones, enzyme substrates, and inhibitors, antibiotics, biological regulators [3]. Their capability to participate in specific biochemical interactions enables the targeted delivery of drug molecules or carrier particles to pathological tissues while minimizing the side effects in other parts of the body. A recent review on protein delivery systems in nanomedicine and tissue engineering emphasized that encapsulation of bioactive molecules needs special attention due to their structural and hence functional sensitivity [4]. Proteins/peptides suffer from metabolic instability, including unfolding, enzymatic degradation, short half-life, and poor bioavailability. To overcome such drawbacks effective protein delivery systems are required to carry and release the therapeutic proteins in a sufficient dose without

*Corresponding author, e-mail: eva.katalin.kiss@ttk.elte.hu

altering their bioactivity. The appropriate carrier construction protects the load from the effects of harsh environments, such as gastrointestinal tracts in the case of most frequently used oral administration. The potential of various colloidal systems applied for oral delivery of bioactive peptides and proteins is overviewed in a recent paper [5]. The size in the nanometer range facilitates their cellular internalization and direct transport of the bioactive substances to the intracellular environment. Polymeric nanoparticles are of special interest since they are more stable than other colloidal carriers, such as liposomes or emulsions, and offer satisfactory protection [6]. The particle surface can be modified by adsorption or chemical coupling of polymers or specific biomolecules to enhance colloidal stability, targeting, adhesion, cellular uptake, and crossing the blood-brain barrier [6–9]. Several successful works have reported the encapsulation of proteins or peptides [10, 11] and the application of novel technologies for hydrophilic molecules [12] in recent years. Nanoprecipitation, as a simple and reproducible method, is the most commonly used preparation technique for producing carrier particles from biocompatible and biodegradable polyesters, such as poly(D,L-lactic acid) (PLA) and poly(D,L-lactic-*co*-glycolic acid) (PLGA) or polycaprolacton (PCL) [13]. Unfortunately, this technique is not suitable for encapsulation of hydrophilic molecules with a few exemptions where the polarity of the drug was modified by variation of pH. The double emulsion technique applicable to hydrophilic compounds, however usually results in larger delivery particles well above the nanometer range [14]. Above all, the main challenge is that the hydrophobic nature of PLGA, PCL, PLA does not provide an optimal surrounding for charged or highly polar peptides/proteins. The mismatch between the polarity of the carrier and the load can contribute to the low entrapment efficiency [15], while the most important consequence is the risk of losing of bioactivity of the encapsulated protein. Reduction of bioactivity of released OVA (ovalbumin) from PLGA NPs by 30–40% was reported previously [16].

These experiences inspired us to propose a nanocarrier providing optimal microenvironment for proteins. A reverse micelle can be considered an ideal compartment, interacting mildly with the hydrated protein. Therefore, special attention should be paid to the development of biocompatible, biodegradable and potent surfactant systems that form reverse micelles, as emphasized by Tonova and Lazarova [17]. A new optimized surfactant system was introduced by Dodevski *et al*. [18] for high-resolution solution NMR of proteins. A binary surfactant mixture of nonionic 1-decanoyl-rac-glycerol and zwitterionic lauryldimethylamine-*N*-oxide (10MAG/LDAO) was identified for protein encapsulation in a low-viscosity medium such as pentane. One of the most desirable features of the system is the high structural fidelity achieved upon encapsulation [19]. Furthermore, the 10MAG/LDAO surfactant combination shows promise as an encapsulation system for therapeutic bioactive molecules, particularly for oral protein delivery [20], due to its ability to preserve the native, functional state of proteins.

Our aim was to develop a nanocarrier system for proteins/peptides with the capability of preserving their structural integrity and possessing the advantageous properties of nanoparticles. To achieve this, we combined the reverse micellar system, which offered exceptional conformational fidelity with nanoprecipitation in a novel two-step procedure. PCL was applied as a carrier polymer since its degradation causes a lower degree of acidification compared to PLGA and PLA. The formation of a reverse micellar system was adapted to the subsequent nanoprecipitation by carefully selecting biocompatible solvents and suitable experimental conditions. In our method, the first step involved the preparation of a reverse nanoemulsion loaded with proteins or peptides, which served as the organic phase for nanoprecipitation in which PCL was dissolved and utilized to form the nanoparticles.

The purified nanoparticle system was characterized by physicochemical methods to determine their size and size distribution, shape, and surface potential. Hen egg white lysozyme and β-lactoglobulin were selected as proteins to test the encapsulation potential of the system. In addition to the drug loading and encapsulation efficiency, *in vitro* protein release was also investigated.

Besides the two proteins, model peptides with different lengths and hydrophilic characteristics were chosen to test the encapsulation. The amount of peptide loading was determined using fluorescence spectroscopy. The peptides included Penetratin and

Transportan, well-studied cell-penetrating peptides. Penetratin is derived from the third helix of the homeodomain of Drosophila Antennapedia protein [21], while Transportan is a chimeric peptide constructed from a 6-residue sequence of the neuropeptide Galanin, a peptide toxin from wasp venom [22]. Alarin, which is an alternative-splicing form of GALP (galanin-like peptide), is involved in a range of normal brain functions and exhibits direct antimicrobial activity [23]. Catestatin is a neuroendocrine peptide with diverse activities, including involvement in inflammatory processes, autoimmune reactions, and direct antimicrobial effect against different bacterial strains [24]. The set of LLRK peptides, on the other hand, are model cationic peptides with different lengths and exhibit antibacterial activity similar to the well-known antimicrobial peptide, Buforin [25].

2. Materials and methods

2.1. Materials

1-decanoyl-rac-glycerol (10MAG) >99% was bought from Avanti Polar Lipids, part of Croda International Plc. (Alabaster, AL, USA). *N*,*N*-dimethyldodecylamine *N*-oxide (LDAO) ≥99.0%, polycaprolactone (PCL) (M_w: ~14 000), and anisole for synthesis were obtained from Sigma-Adrich Kft (Merck KGaA, Darmstadt, Germany), while polyvinyl alcohol (PVA) ELVANOL grade 51-05, (M_w: ~25 000) from Dupont de Nemours & amp; Co. (Wilmington, Delaware, USA), and ethyl formate 98+%, pure from Acros Organics part of Thermo Fisher Scientific (Waltham, MA, USA).

Hen egg white lysozyme (>95%) with a molecular weight of 14 300 was purchased from VWR International Kft. (Debrecen, Hungary), while β-lactoglobulin AB (>90%) with a molecular weight of 18 400 was obtained from Sigma-Aldrich Kft. (Budapest, Hungary). The protein concentration was determined using the ML Protein Assay, a modified protein assay based on Lowry's Method, which was obtained from G-Biosciences, Geno Technology, Inc. (St. Louis, MO, USA). The components of the kit include Folin's reagent, copper solution, reagent D, and a BSA protein standard (2 mg/ml).

For peptide synthesis, Fmoc-amino acid derivatives were obtained from Iris Biotech (Marktredwitz, Germany). Fmoc-Rink Amide MBHA resin, 5(6)-carboxyfluorescein (Cf), *N*,*N*′-diisopropylcarbodiimide (DIC), 1-hydroxybenzotriazole (HOBt), 1,8-diazabicyclo[5.4.0]undec-7-ene (DBU), and triisopropylsilane (TIS), were obtained from Merck (Budapest, Hungary). Trifluoroacetic acid (TFA), *N*,*N*-dimethylformamide (DMF), dichloromethane (DCM), diethyl ether, piperidine, and acetonitrile (AcN) were from VWR (Budapest, Hungary).

For the biological assays, RPMI-1640 medium, phosphate-buffered saline (PBS, pH = 7.4), 2 mM L-glutamine and trypan blue were from Lonza (Basel, Switzerland), while trypsin, penicillin-streptomycin were from Gibco (Thermo Fisher Scientific, Waltham, MA, USA). Fetal bovine serum (FBS) was from EuroClone (Pero, Itlay). Resazurin sodium salt was from Merck (Budapest, Hungary).

2.2. Peptide synthesis, purification, and characterization

Peptides were prepared on solid phase (150 mg Fmoc-Rink Amide MBHA resin, capacity = 0.39 mmol/g) in an automated peptide synthesizer (Syro-I, Biotage, Uppsala, Sweden) using Fmoc/tBu strategy with DIC/HOBt coupling reagents as described earlier [26, 27].

For the fluorescent labeling, 5(6)-carboxyfluorescein was coupled on the *N*-terminus of the peptides using DIC/HOBt coupling reagents, similarly to the method presented previously [26]. After the synthesis was completed, peptides were cleaved from the resin with TFA in the presence of scavengers (H_2O and TIS, 3-3 v/v%). Crude products were precipitated in cold diethyl ether, centrifuged (4000 rpm, 5 min), and lyophilized from H_2O/AcN. Cf-labelled peptides were then purified by RP-HPLC on a Phenomenex Jupiter Proteo C12 column (10 μm, 90 Å, 10×250 mm) with linear gradient elution using 0.1% TFA in H_2O (eluent A) and 0.1% TFA in AcN:H_2O = 80:20 v/v (eluent B) on an UltiMate 3000 Semiprep HPLC (Thermo Fisher Scientific, Waltham, MA, US). Purified peptides were analyzed by RP-HPLC using a LC-40 HPLC System (Shimadzu, Kyoto, Japan) on an analytical Phenomenex Jupiter Proteo C12 column (10 μm, 90 Å, 4.6×150 mm). The flow rate was 1 ml/min, the gradient was 5–100 B% in 20 min (UV detection at λ = 220 nm). High-resolution mass spectrometry was performed on a Thermo Scientific (Waltham, MA, USA) QExactiv Focus Hybrid Quadrupole-Orbitrap Mass Spectrometer. The main

Table 1. Main physico-chemical properties of Cf-peptides.

	Peptide sequence	M_{mo} (calculated)[1]	M_{mo} (measured)[2]	pI[3]	Rt HPLC[4] [min]	Z[5]	H[6]
Cf-Penetratin	RQIKIWFQNRRMKWKK	2602.3532	2602.3544	12.81	15.9	7+	–8.75
Cf-Transportan	AGYLLGKINLKALAALAKKIL	2538.4614	2538.4631	10.66	17.1	4+	1.19
Cf-Catestatin	SSMKLSFRARAYGFRGPGPQL	2682.2802	2682.2766	12.22	12.5	4+	–4.57
Cf-Alarin	APAHRSSTFPKWVTKTERGRQPLRS	3249.6220	3249.6163	12.51	11.2	6+	–9.93
Cf-L1	LLRK	885.4379	885.4371	11.54	14.9	2+	–1.84
Cf-L2	LLRKLLRK	1395.8021	1395.8006	12.52	13.4	4+	–3.68
Cf-L3	LLRKLLRKLLRK	1906.1664	1906.1644	12.81	16.9	6+	–5.52
Cf-L4	LLRKLLRKLLRKLLRK	2416.5306	2416.5272	12.99	18.4	8+	–7.36

[1]Theoretical molecular mass was calculated with Thermo Xcalibur 3.1 Qual Browser software.
[2]Monoisotopic molecular mass was measured on a Thermo Scientific (Waltham, MA, USA) QExactiv Focus Hybrid Quadrupole-Orbitrap Mass Spectrometer. The deviation of the measured mass from the theoretical mass of the peptides (ΔM) was always lower than 4 ppm.
[3]Theoretical pI was calculated with the use of ProtParam analysis tool (Expasy) [28]
[4]Retention time on analytical HPLC chromatograms, using 5–100 B% in 20 min gradient elution on a Phenomenex Jupiter Proteo C12 column (10 µm, 90 Å, 4.6×150 mm).
[5]Charge of side chains at neutral pH
[6]Calculated from hydrophobicity of amino acids [29]

physico-chemical properties of the Cf-peptides are shown in Table 1.

2.3. Preparation of nanoparticles

A two-step procedure was developed for the nanoencapsulation of proteins and Cf-peptides. Firstly, a reverse nanoemulsion was formed, followed by processing this nanoemulsion in a nanoprecipitation procedure.

Due to the hygroscopic nature of LDAO, it was dried at 60 °C and −0.1 mbar for 3 h before use. A solution of 10MAG:LDAO in a 65:35 w/w ratio, with a total concentration of 0.8 M, was prepared in anisole:ethyl formate at 1:1v/v ratio. The solution was filtered using a 0.25 µm syringe filter. At this point, PCL was dissolved in the organic phase to a concentration of 10 g/l. The nanoemulsion was prepared by adding 85 µl of the protein or Cf-peptide solution in water (loading concentration) to 1 ml of the organic solution. The mixture was sonicated for 1 min at 30 W and 30% pulse settings with an ultrasonic homogenizer model 150vt from BioLogics Inc. (Manassas, VA, USA) while cooling the sample in ice bath.

A 1 % aqueous solution of PVA, filtered using a 0.25 µm syringe filter, was used as a stabilizer in the nanoprecipitation. 1 ml of the nanoemulsion was added to 3.35 ml of the stabilizer solution with an automatic syringe, and the system was stirred for one hour.

The particles obtained from the nanoprecipitation were purified by centrifugation. The sol was centrifuged at 3000 rpm for 10 min to remove possible particle aggregates (Boeco S8, Boeckel+Co, Hamburg, Germany). The sol was separated and further centrifuged at 12 000 rpm for 20 min (Hettich Mikro 200R, Andreas Hettich GmbH & Co. KG Tuttlingen Germany), the supernatant was removed and the pellet containing the particles was redispersed in double distilled water. This purification procedure was repeated three times.

2.4. Characterization of nanoparticles

Dynamic light scattering (DLS) was used to characterize the average size and size distribution of the nanoparticles. The Nanolab 3D instrument from LS Instruments (Switzerland) was used for the DLS measurements. The radius of both nanoemulsion and polymer particles was measured at 25.0±0.1 °C, and the results were collected 5 times. After sonication, the nanoemulsion was allowed to rest for 3 h for thermal equilibration before measuring the droplets' radius. The radius of the nanoparticles was taken immediately after purification.

The stability of the PCL nanoparticle sol was investigated by storing it at a temperature of 4 °C. The change in particle size was monitored by DLS.

Atomic force microscopy (AFM) was used to study the appearance and morphology of nanoparticles. Samples were prepared on freshly cleaved, highly

oriented pyrolytic graphite (HOPG) surfaces. A total of 50 µl of the particle sols were equilibrated on the HOPG surface for 15 min to allow for sorption and interaction between the particles and the substrate. The excess liquid was then carefully aspirated, and the samples were dried under vacuum to ensure the removal of any residual solvent. AFM imaging was performed using a Nanosurf FlexAFM instrument (Nanosurf AG, Switzerland) operating in dynamic mode utilizing Tap190-GD probes from BudgetSensors (Bulgaria). The acquired AFM images were further processed and analyzed using the Gwyddion software, converting the recorded data into 3D topographical maps.

The electrophoretic mobility of the samples was determined by Zetasizer Nano Z (Malvern Panalytical) apparatus at 25.0±0.1 °C. Results were collected in triplicate. The zeta potential (ζ) was calculated from the electrophoretic mobility values using the Smoluchowski approximation. Zeta-potential measurements were repeated at least three times, and average values were given with the standard error of the mean (SEM).

The amount of encapsulated protein was determined in a direct way using Lowry's method. Nanoparticles were incubated in 0.05 M NaOH for 24 h at 37 °C. 25 µl of protein solution was mixed with reagent D and the copper solution. Folin's reagent was added to the mix, vortexed for a few seconds, and after 30 min the absorbance at 750 nm was measured. The concentration was determined using a calibration curve. 1 ml of particle sol was lyophilized and weighed to calculate the drug loading (DL). Encapsulation efficiency (EE) was expressed as the ratio of encapsulated protein to the total protein loaded into the system.

Cf-labelled peptides were encapsulated and used for calculating the concentration of the peptides loaded in the nanoparticle formulation. Fluorescence spectra were recorded using a VARIAN Cary Eclipse (Agilent Technologies Inc.) fluorescence spectrophotometer (right angle geometry, 1×1 cm quartz cell). The temperature (25.0±0.1 °C) in the cuvette was controlled by a Peltier-type thermostat. Spectra of encapsulated peptides and pure ones were compared to calculate the concentrations. The excitation wavelength was set at 230 nm, and the scan range was from 250 to 700 nm with 5 nm monochromator slits.

2.5. *In vitro* release from nanoparticles

The protein release rate from the nanoparticles was determined using a dissolution test conducted at 37 °C in a water bath under continuous stirring. Appr. 5 mg of NPs was incubated in 10 ml of phosphate-buffered saline (PBS) as release medium. At fixed time intervals, a 1 ml sample was withdrawn, and the amount of released protein was determined by Lowry test from the supernatant after centrifugation at 12 000 rpm for 20 min. Following each sampling, the withdrawn sample was replaced by the sediment dispersed in fresh PBS.

Various experimental models for describing drug release kinetic were applied to reveal the release mechanism.

The Gompertz model is a simple exponential model suitable for burst release profiles where the released drug amount converges to a maximum value. The model is described by Equation (1):

$$\frac{c_t}{c_0} = C_{max} \cdot \exp\left[-a \cdot e^{b \log t}\right] \quad (1)$$

where C_{max} is the maximum dissolution of the drug, a determines the undissolved proportion at time $t = 1$ and is described as the location parameter, while b is the shape parameter, describing the dissolution rate [30].

The Korsmeyer-Peppas model can be used for polymeric systems to determine the release mechanism by fitting the initial part of the release profile with Equation (2):

$$\frac{c_t}{c_0} = k \cdot t^n \quad (2)$$

where c_t is the cumulative amount of released drug up to t time, c_0 is the total drug content, k is the release rate constant, and n is the release exponent. The value of n is used to differentiate between release mechanisms [31].

The Peppas-Sahlin model (Equation (3)) was also used to approximate the contributions of different mechanisms in the overall release profile:

$$\frac{c_t}{c_0} = K_1 \cdot t^m + K_2 \cdot t^{2m} \quad (3)$$

where K_1 and K_2 are the contributions of the Fickian and case II mechanisms. Here the Fickian mechanism means a purely diffusion-controlled release, while the case II mechanism describes the swelling-triggered relaxation of the polymer matrix resulting in a steady release of the encapsulated material. The constant m is 0.43 for spherical particles [32].

2.6. Cytotoxicity

For the viability assay, MonoMac-6 (MM6) human monocytic cells [33, 34] (DSMZ no.: ACC 124) were maintained as an adherent culture in RPMI-1640 media, supplemented with 10% FBS, 2 mM L-glutamine, and penicillin-streptomycin mixture (50 IU/ml and 50 µg/ml, respectively) and CellCultureGuard (PanReacApplichem) at 37 °C in a humidified atmosphere containing 5% CO_2. Cells were seeded in a 96-well tissue culture plate (Sarstedt, $1 \cdot 10^4$ cells in 100 µl complete medium) one day before the experiment. Cells were then treated with the empty and protein or Cf-peptide-loaded nanoparticles in serum-free media for 24 h. After centrifugation (1000 rpm, 5 min) and washing with serum-free media, cell viability was measured by adding 22 µl (10% v/v) Alamar Blue reagent solution (Resazurin sodium salt, 0.15 mg/ml, dissolved in PBS, pH 7.4) [35]. After 2 h of incubation, the fluorescence was detected (λ_{Ex} = 530/30 and λ_{Em} = 610/10 nm) in a Synergy H4 multimode microplate reader (BioTek, Winooski, VT, USA). All measurements were performed in quadruplicate, and the mean viability, compared to the untreated control, was presented together with ± SEM.

Parallel with the Alamar Blue assay, images of the cells were captured after 24 h of treatment with an Olympus CKX41 microscope (objective: 40X).

3. Results and discussion

3.1. Characterization of nanoparticles

The reverse nanoemulsion was prepared in an organic medium consisting of a 1:1 mixture of anisole and ethyl formate, using a surfactant mixture composed of the nonionic 10MAG and zwitterionic LDAO. The 10MAG/LDAO surfactant composition was selected based on a suggestion from a recent report [18]. A novel organic solvent, different from the previously used alkanes, needed to be identified that would be both biocompatible and non-toxic. After several trials, the anisole/ethyl formate mixture proved to be a suitable solvent for the surfactants, becoming the outer phase of reverse nanoemulsion. Aqueous nanodroplets were formed with an average radius of 6 nm (Table 2). The system did not form spontaneously but showed satisfactory stability

Table 2. Size of unloaded and protein or Cf-peptide loaded reverse nanoemulsion droplets, r_{ne} and corresponding nanoparticles, r_{NP} determined by DLS at various loading concentrations, c, as well as the zeta-potential (ζ) values of nanoparticles.

Protein	c [g/l]	Nanoemulsion		Nanoparticles		
		r_{ne} [nm]	PDI	r_{NP} [nm]	PDI	ζ [mV]
–	–	6.0±0.7	0.55±0.06	180±8	0.23±0.05	–11.0±0.7
Lysozyme	0.5	9.2±0.7	0.30±0.04	183±9	0.17±0.05	0.5±0.3
	1.0	7.5±0.4	0.50±0.07	202±2	0.28±0.02	7.0±0.7
	4.0	11.8±0.2	0.40±0.01	214±9	0.20±0.10	4.6±0.6
β-lactoglobulin	0.5	9.3±0.4	0.30±0.06	245±14	0.20±0.10	2.5±0.1
	1.0	8.9±0.9	0.50±0.04	223±6	0.27±0.03	8.0±0.2
	4.0	13.4±0.6	0.80±0.07	202±6	0.18±0.05	5.4±0.3
Cf-peptide						
Cf-Penetratin	0.02	13.7±0.5	0.40±0.10	208±45	0.20±0.10	20.1±0.8
Cf-Transportan	0.02	10.0±0.3	0.30±0.10	290±23	0.28±0.08	5.2±0.5
Cf-Catestatin	0.02	12.0±1.0	0.70±0.30	186±3	0.28±0.02	15.4±0.5
Cf-Alarin	0.02	15.0±1.4	0.70±0.10	151±1	0.20±0.03	23.0±1.0
Cf-L1	0.02	10.6±0.8	0.46±0.04	170±2	0.24±0.01	21.0±4.0
Cf-L2	0.02	9.0±0.4	0.42±0.03	239±7	0.27±0.02	33.0±3.0
Cf-L3	0.02	6.4±0.3	0.52±0.03	168±30	0.25±0.09	23.0±3.0
Cf-L4	0.02	10.8±0.5	0.23±0.05	142±2	0.21±0.02	43.0±4.0

following sonication, allowing for further procedures. Anisole was an important component of the solvent mixture since it is an especially good solvent of PCL [36], the material used for polymer coating. Both anisole and ethyl formate belong to the residual solvent Class 3, according to the US Pharmacopeia [37], and they present no human health hazards at levels normally accepted in pharmaceuticals.

The loading of proteins or Cf-peptides resulted in a noticeable increase in the size of the aqueous nanodroplets. The typical diameter of these peptide-containing nanodroplets is 10–15 nm, depending on the type of protein/peptide and possibly on the amount of loading of the droplets compared to the blank one with radius of 6 nm.

These reverse nanoemulsions were used as the organic phase in the subsequent nanoprecipitation process. It was introduced under continuous stirring to the aqueous solution of the stabilizer (PVA). This resulted in the formation of an aqueous dispersion of PCL-coated particles, where the proteins or Cf-peptides were contained within the particle core with hydropilic microenvironment. The size data of nanoparticles loaded with lysozyme, β-lactogobulin, Cf-peptides, and a reference sample without peptides are presented in Table 2.

The radius of nanoparticles formed without protein or Cf-peptide loading was found to be 180 nm with good reproducibility. Their loading with proteins results in a significant increase in size, except in the case of the lowest concentration of lysozyme. The polydispersity, similar to the unloaded system, is about 0.2–0.3, which indicates a relatively narrow size distribution. Loading with Cf-peptides did not show a clear tendency in size change, although the average radius seems to increase compared to the blank particles, except in two cases. The size of all protein/Cf-peptide loaded nanoparticles remained below 500 nm in diameter. Peptide loaded nanoparticles show size distribution $0.2 < PDI < 0.3$.

AFM images were collected on unloaded and protein-loaded nanoparticles (Figure 1). The images reveal roughly spherical nanoparticles, with the unloaded particles appearing smaller (200–300 nm in diameter) compared to the protein-loaded particles (300–500 nm). The larger size of the protein-loaded particles suggests the incorporation of proteins into the nanoparticles. The observed sizes correlate with the measurements obtained by DLS, although the slightly smaller sizes may be attributed to the dry state of the particles during AFM imaging.

The zeta-potential of unloaded PCL nanoparticles is a small negative value (−11 mV), as expected, indicating the presence of negatively charged end-groups of the PCL chains that are partially shielded by the surface PVA layer. The protein-loaded nanoparticles showed a somewhat modified zeta-potential,

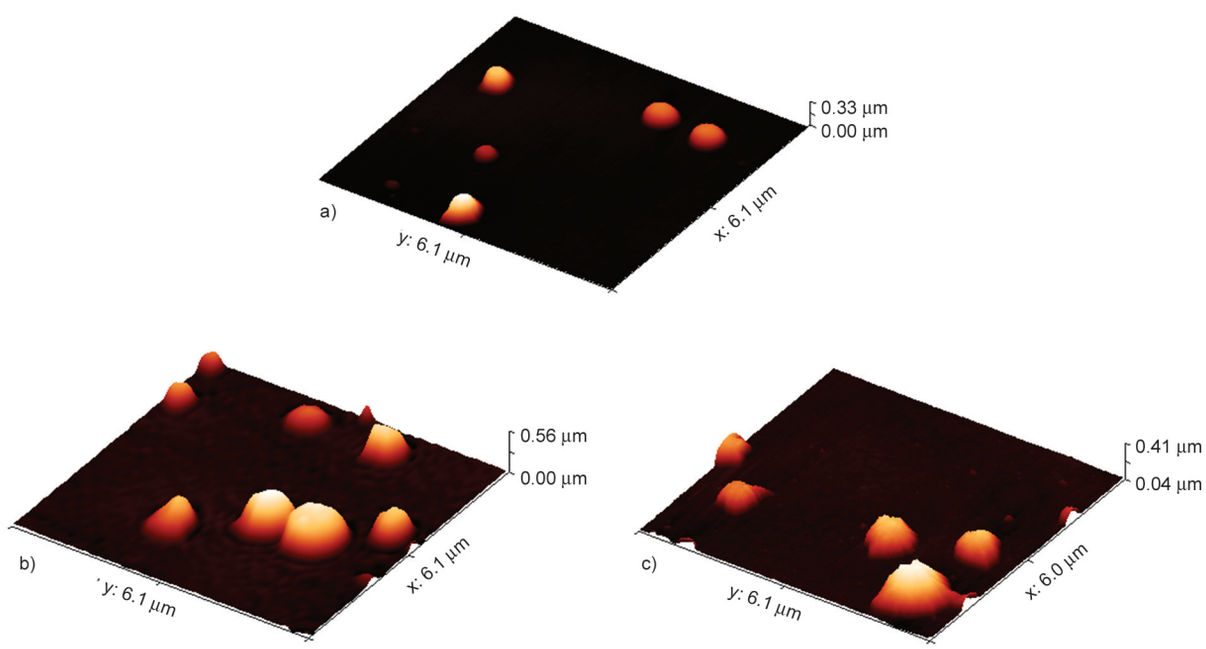

Figure 1. AFM topography images of unloaded (a), lysozyme (b) and β-lactoglobulin (c) loaded nanoparticles.

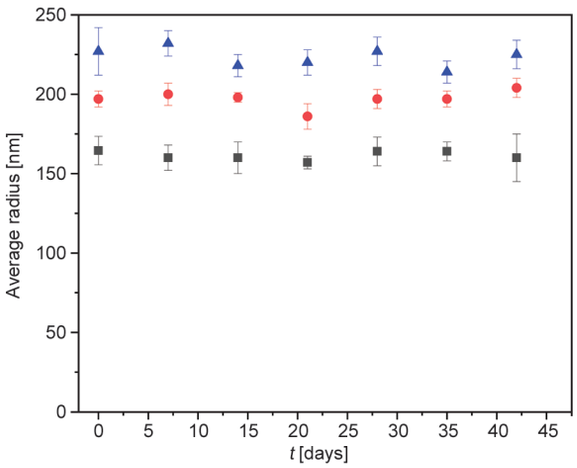

Figure 2. Average particle size determined by DLS of unloaded (■), lysozyme (●) and β-LG (▲) loaded particles during the storage.

falling within the range of 0 to +8 mV. Similarly, reduced zeta-potential was measured and analyzed for ovalbumin encapsulation into PEG or PEG-*b*-PAGE modified polymeric nanoparticles [16]. A more evident charge reversal was observed, however, in the cases of Cf-peptide-loaded nanoparticles, with zeta-potential varying between +5 and +43 mV. This finding suggests that in addition to encapsulation, some peptide molecules are bound to the surface of NPs. Adsorption of the highly charged cationic peptides is favoured by the negatively charged surface of NPs. This electrostatic interaction leading to positive zeta-potential seems to be most effective for peptides with high specific charge (charge related to the number of amino acids) above 0.4, while it is weakest for Cf-Transportan and Cf-Catestatin, which have the smallest specific charges of 0.19 and 0.24, respectively.

The storage stability investigation of the drug delivery system showed that the average radius of the particles, either unloaded or protein-loaded did not change significantly, with the variation remaining within the range of the SEM over one month (Figure 2).

The concentration of the purified nanoparticle system was 1.12±0.20 mg/ml, with a yield of about 50%, similarly to values reported previously [38–41]. The success of protein encapsulation into nanoparticles was characterized by their protein content, measured as drug loading (DL) and encapsulation efficiency (EE). These results are presented in Figure 3. For lysozyme, the DL values showed a significant increase from 10 to 60 μg/mg with loading concentration in the range of 0.5–4.0 g/l. The corresponding EE did not exhibit a clear dependence on loading concentration and remained at approximately 10%. In contrast, the β-LG encapsulation presents a different behaviour. The DL values are quite high, ranging from 60 to 40 μg/mg. Although the initial EE at low protein concentration is impressive, >60%, a drastic decrease is observed at higher concentrations. Consequently, to achieve high DL, it is satisfactory to use low β-LG loading concentration. In contrast, for lysozyme, a notable increase in loading concentration is required to reach high DL.

This opposing behaviour of the two proteins can be analysed considering their molecular properties. Their molecular weights are in a similar range but due to their amino acid composition, they are characterized

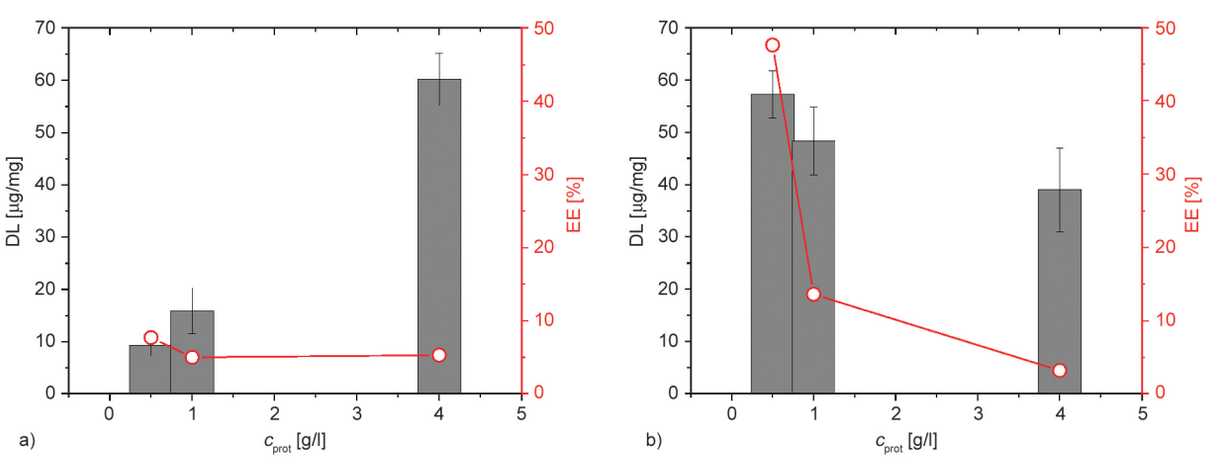

Figure 3. Lysozyme (a) and β-lactoglobulin (b) content (DL) of nanoparticles and the corresponding encapsulation efficiency values (EE) at various protein loading concentrations (c_{prot}).

by quite different isoelectric points (pI) with values of 10.7–11.1 for lysozyme and 5.4 for β-LG [42]. Upon encapsulation in reverse nanoemulsions, the proteins are located in the aqueous interior of surfactant micelles. The pH of this nanoscale water core is crucial to consider the charge state of protein molecules and their potential interactions. A sensitive method for measuring pH of the 10MAG/LDAO reverse micelle aqueous interior was developed using one-dimensional ^{1}H and two-dimensional heteronuclear NMR spectroscopy [43]. Amide nitrogen and amide hydrogen chemical shifts of ubiquitin, a 8.5 kDa protein, were used as the indicator of pH environment. The effective pH of the 10MAG/LDAO core was found to be 7, primarily influenced by the surfactant mixture. The net charge of lysozyme is +4 at pH 7 [44] supported by positive zeta-potential values of 4.1±0.7 mV [42, 45]. On the other hand, the net charge of β-LG is −8 [46], consistent with the negative zeta-potential determined previously as −26.9±0.7 mV [47]. Consequently, electrostatic repulsion between the protein molecules is expected in both cases, providing unfavourable conditions for their accumulation in the core of the nanodroplet. However, the experimental finding for β-LG encapsulation (Figure 3) contradicts this expectation, showing high drug loading even at low concentrations.

Further examination of the charge properties of proteins through molecular dynamic simulations revealed that the electrostatic potential contours are highly asymmetric for β-LG [48], while lysozyme shows a lower degree of patchiness [49]. The well-defined asymmetry of charge and potential distribution of β-LG surface leads to attractive forces between the positive and negative domains of associating proteins, aiding in understanding the pH-dependent aggregation behaviour of that protein [46, 50]. This structural peculiarity, coupled with β-LG's high

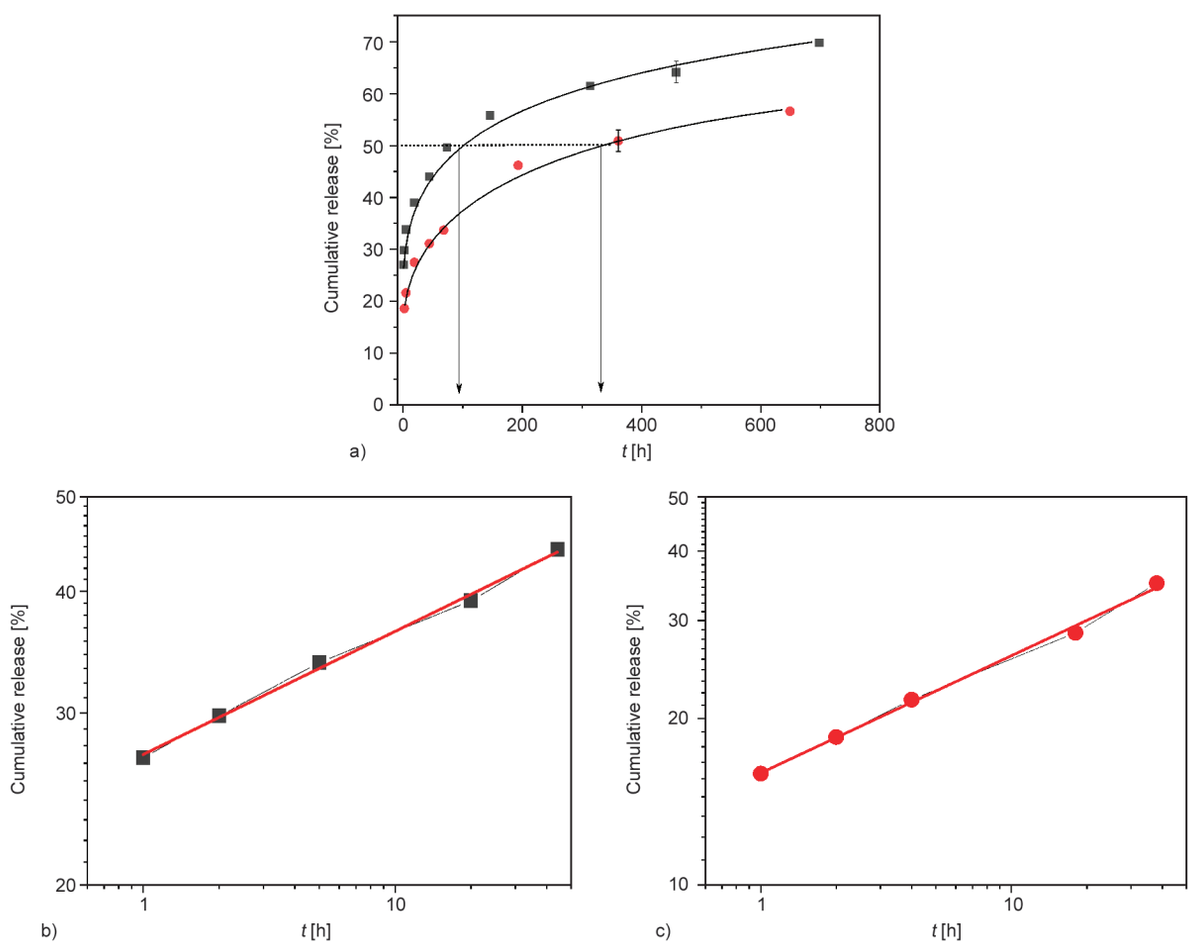

Figure 4. *In vitro* lysozyme (■) and b-lactoglobulin (●) release from nanoparticles. (The lines are guided to the eyes) Each data point represents the mean of three determinations. Figure 4b and c show the fitting of Korsmeyer-Peppas model for the initial part of the experimental data.

affinity to bind hydrophobic ligands, might explain its ability to accumulate preferably in the reverse micellar core of the nanoemulsion.

The dissimilar surface charge distribution of the two proteins, which is responsible for the difference in molecular interactions, might result in either effective or less favoured encapsulation. It appears that the given nanoemulsion system has a maximum loading capacity for proteins, which is fully utilized over the entire concentration range for β-LG and only at the highest concentration for lysozyme.

Cf-peptide content of nanoparticles was determined by fluorescent spectroscopy using a direct method, where the amount of encapsulated Cf-peptide was measured and found to be in the micromolar range.

3.2. *In vitro* release

The release of proteins from nanoparticles was investigated for one month. Figure 4 shows the *in vitro* release profile of lysozyme and β-lactoglobulin in PBS at 37 °C. The cumulative released amount as a function of time reflects a biphasic release profile with an initial period of high release rate followed by a significant reduction and nearly steady release up to 700 h. The release rate of β-lactoglobulin is lower than that of lysozyme throughout the investigated period. 20% of the encapsulated β-LG was released in the first 2 h, while this value was 30% for lysozyme. Notably, the half-life values are 94 h for lysozyme and 330 h for β-lactoglobulin.

Various release kinetics models, including Gompertz, Peppas-Sahlin, and Korsmeyer-Peppas, were employed to describe the release behavior. The kinetics of protein release is well described by the Korsmeyer-Peppas model in the first 40 h, with a correlation coefficient (R^2) of 0.983 and 0.995 for lysozyme and β-LG, respectively. The k parameter in the equation, which describes all the geometrical and structural characteristics of the matrix, was 26.3 for lysozyme and 15.9 for β-LG. The n parameters, related to the mechanism that governs the release kinetics, were found to be quite low, 0.13 and 0.21 for lysozyme and β-LG, respectively. For spherical particles, if $n < 0.43$, the mechanism can be considered quasi-Fickian diffusion-controlled ($n = 0.43$ corresponds to Fickian diffusion), where the rate of release is mostly dependent on the diffusion of the drug in the polymer matrix. These low n values observed here are the indication of greatly hindered diffusion leading to favorable extended release.

The overall release process exhibits an initial burst release followed by sustained release of the encapsulated protein. According to the classification presented in a recent release analysis [51], this profile can be produced by core-shell particles where two compartments are defined, and the active substance is transported through these with two distinct apparent diffusion coefficients. The inner core of the capsule initially contains the homogeneously distributed active substance characterized by $D_{core} > D$ (to mimic a liquid core). An example of such a system is described as a release reservoir by Nordstierna *et al*. [52], where the active component is localized in a spherical core and coated with a polymeric matrix. The obtained release pattern suggests that the nanoparticles prepared using reverse nanoemulsions have possibly formed core-shell structures. This type of structure can contribute to the sustained release observed in this study. The ability to achieve sustained release from these nanoparticles may have potential applications in specific fields where prolonged drug delivery is desired.

3.3. *In vitro* biological investigations

Cytotoxicity of the empty NP and peptide-loaded NPs was measured on MonoMac-6 human monocytes. After 24 h of treatment, empty NP was not toxic to the cells. Similarly, Catestatin- and Alarin-loaded NPs were also not cytotoxic (Figures 5a, 5c). NP-Penetratin showed the highest toxicity, and this effect was more pronounced than the cytotoxicity of the free Penetratin peptide (Figure 5b). Marked membrane disruption was visualized on the microscopic images of NP-Penetratin-treated cells (Figure 5c). Membrane integrity is critical for cell survival, defects of which cause leakage and, finally, cell death. Cytotoxicity of the free peptides obtained is in line with earlier results described previously [26, 53].

Besides cationic cell-penetrating and antimicrobial peptides, a set of sequential oligopeptides containing a repetitive LLRK motif was also assessed (Figure 6). The viability of cells treated with L1-L4 peptide-loaded NPs was always higher than 60%, although higher toxicity was measured for NP-particulated peptides than free peptides (Figure 6b). On the

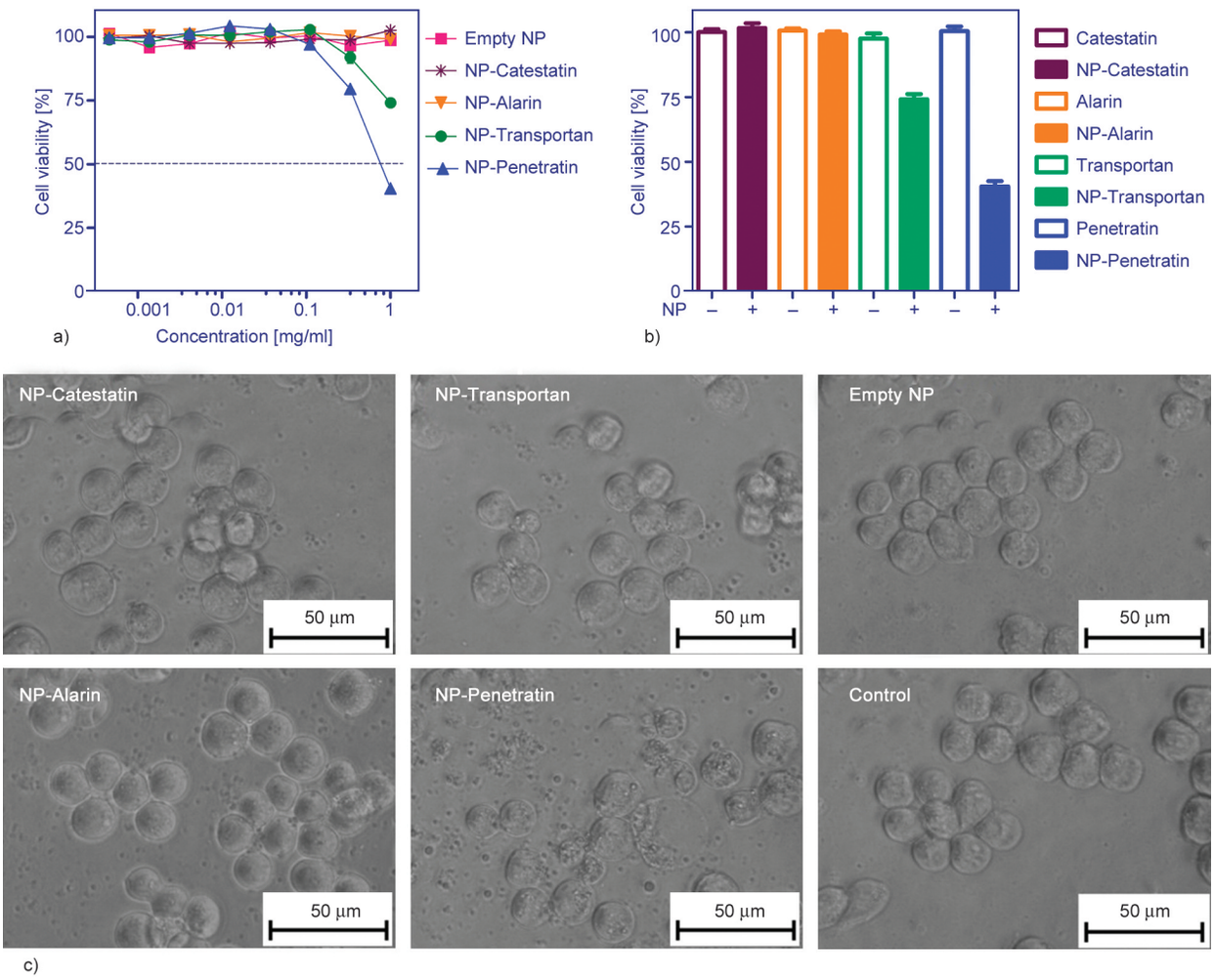

Figure 5. Assessment of cell viability. MonoMac-6 human monocytes were treated with empty NP and peptide-loaded NPs for 24 h, and the cell viability was measured with Alamar Blue assay (a). The cytotoxicity of NP-encapsulated peptides was compared with the cytotoxicity of the free peptides (1 µM peptide concentration (b). After 24 h of incubation, NP-peptide-treated cells were captured with an Olympus CKX41 microscope (objective: 40×) (c). Membrane damage caused by NP-Penetratin is visible on the microscopic image.

microscopic images, only slight membrane damage was visible in the case of NP-L4 (Figure 6c).

Proteins as drug candidates are also important groups of compounds; therefore, we have investigated two proteins' encapsulated constructs. The cytotoxic effect of the nanoparticulated β-lactoglobulin AB (NP-BLG) and hen egg white lysozyme (NP-Lys) was assessed as well (Figure 7). None of the particles showed cytotoxicity on MonoMac-6 cells up to the highest concentration (0.3 mg/ml).

4. Conclusions

The development of protein and peptide-based therapeutic agents has never been as active as it is today, leading to an increasing number of approved drugs and diagnostic reagents. These compounds, however, are tempered by certain limitations: short lifetime due to enzymatic degradation and immune response, poor bioavailability, and low permeability. Research is dynamic in the rational design of structure-activity but also formulation platforms to eliminate these drawbacks. Novel nanoencapsulation strategies employing biodegradable and polymeric carriers allow for the modulation of pharmacokinetic properties and target specificity of peptide- and protein derivatives. The novel combined encapsulation method introduced can be a favourable approach to delivering hydrophilic peptides/proteins since it applies a special nonionic/ zwitterionic surfactant mixture for stabilization of nanoemulsion that proved to be advantageous in preserving their conformational properties. The subsequent nanoprecipitation process

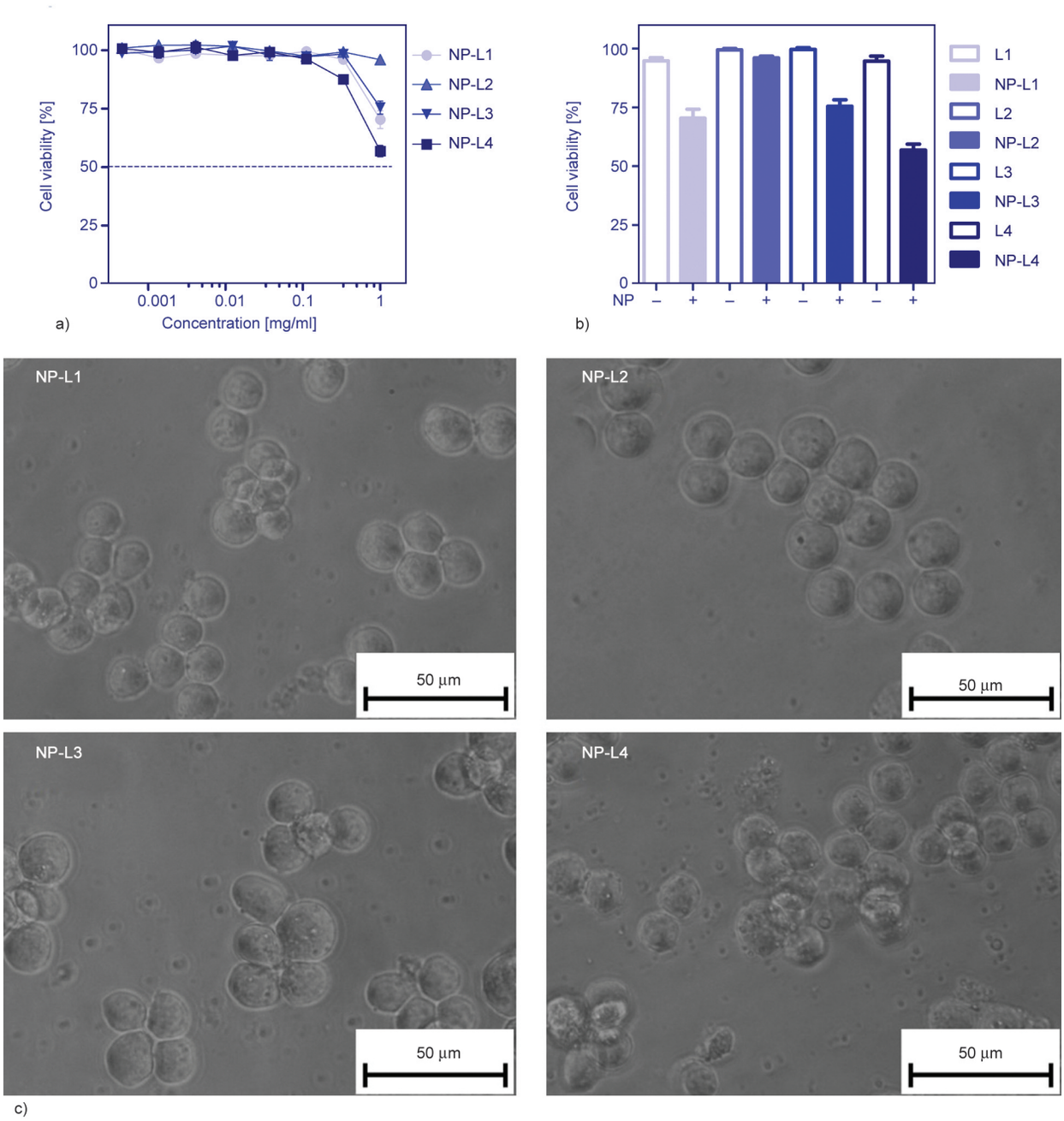

Figure 6. Cytotoxic effect of NP-Lx peptide set. Viability of MonoMac-6 human monocytes after treatment with NP-Lx peptides for 24 h (a). Comparison of free Lx peptides and NP-encapsulated analogues in terms of cytotoxicity (b). Microscopic images do not show significant membrane damage on NP-Lx treated cells (c).

resulted in polymeric nanoparticles dispersible in aqueous medium and hence allowed easy handling of the system (storage, lyophilization) while providing the possibility of surface functionalization. The results presented here show the first experiences of loading that nanoencapsulation system with a set of cell-penetrating peptides and two model proteins. The physico-chemical characterization, *in vitro* release, and cytotoxicity results of protein-loaded nanoparticles appear promising, while the encapsulated membrane-active peptides exhibited increased bioactivity. Further experiments, exploring the molecular interactions between the encapsulated material and the carrier substance, as well as the effects of the particle's inner structure on bioactivity, can contribute to the rational design of carrier systems with optimized performance.

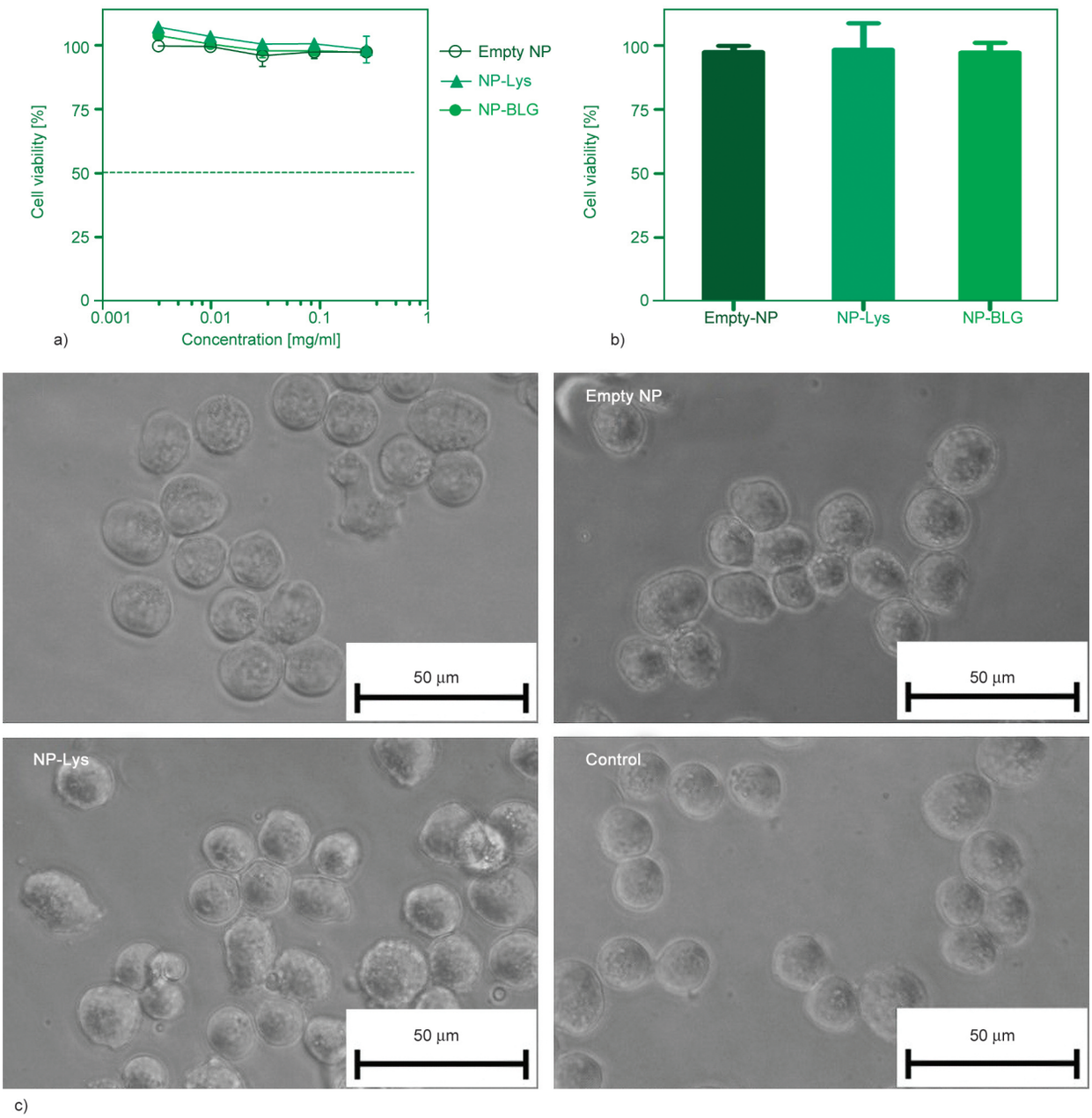

Figure 7. Cytotoxic effect of nanoparticulated β-lactoglobulin AB (NP-BLG) and hen egg white lysozyme (NP-Lys). Mono-Mac-6 human monocytes were treated with empty NP and NP-proteins (a). Cell viability, measured at the highest treatment concentration (0.3 mg/ml NP) is presented in panel (b), while microscopic images of the cells are in panel (c).

Acknowledgements

Financial support of National Research, Development and Innovation Office, Hungary (NKFIH Grant No. 142904, Grant No. 142754 and VEKOP-2.3.3-15-2017-00020) is gratefully acknowledged. This work has been implemented with the support provided by the National Research, Development, and Innovation Fund of Hungary (Project no. 2018-1.2.1-NKP-2018-00005), by the Momentum Program (LP2021-28) of the Hungarian Academy of Sciences, and by the ELTE Thematic Excellence Programme 2020 (Szint+).

References

[1] Wang L., Wang N., Zhang W., Cheng X., Yan Z., Shao G., Wang X., Wang R., Fu C.: Therapeutic peptides: Current applications and future directions. Signal Transduction and Targeted Therapy, **7**, 48 (2022). https://doi.org/10.1038/s41392-022-00904-4

[2] Berillo D., Yeskendir A., Zharkinbekov Z., Raziyeva K., Saparov A.: Peptide-based drug delivery systems. Medicina, **57**, 1209 (2021). https://doi.org/10.3390/medicina57111209

[3] Tesauro D., Accardo A., Diaferia C., Milano V., Guillon J., Ronga L., Rossi F.: Peptide-based drug-delivery systems in biotechnological applications: Recent advances and perspectives. Molecules, **24**, 351 (2019). https://doi.org/10.3390/molecules24020351

[4] Bizeau J., Mertz D.: Design and applications of protein delivery systems in nanomedicine and tissue engineering. Advances in Colloid and Interface Science, **287**, 102334 (2021). https://doi.org/10.1016/j.cis.2020.102334

[5] Perry S. L., McClements D. J.: Recent advances in encapsulation, protection, and oral delivery of bioactive proteins and peptides using colloidal systems. Molecules, **25**, 1161 (2020). https://doi.org/10.3390/molecules25051161

[6] des Rieux A., Fievez V., Garinot M., Schneider Y-J., Préat V.: Nanoparticles as potential oral delivery systems of proteins and vaccines: A mechanistic approach. Journal of Controlled Release, **116**, 1–27 (2006). https://doi.org/10.1016/j.jconrel.2006.08.013

[7] Kasza G., Gyulai G., Ábrahám Á., Szarka G., Iván B., Kiss É.: Amphiphilic hyperbranched polyglycerols in a new role as highly efficient multifunctional surface active stabilizers for poly(lactic/glycolic acid) nanoparticles. RSC Advances, **7**, 4348–4352 (2017). https://doi.org/10.1039/C6RA27843D

[8] Horváti K., Gyulai G., Csámpai A., Rohonczy J., Kiss É., Bősze Sz.: Surface layer modification of poly(D,L-lactic-*co*-glycolic acid) nanoparticles with targeting peptide: A convenient synthetic route for pluronic F127–tuftsin conjugate. Bioconjugate Chemistry, **29**, 1495–1499 (2018). https://doi.org/10.1021/acs.bioconjchem.8b00156

[9] Monge M., Fornaguera C., Quero C., Dols-Perez A., Calderó G., Grijalvo S., García-Celma M. J., Rodríguez-Abreu C., Solans C.: Functionalized PLGA nanoparticles prepared by nano-emulsion templating interact selectively with proteins involved in the transport through the blood-brain barrier. European Journal of Pharmaceutics and Biopharmaceutics, **156**, 155–164 (2020). https://doi.org/10.1016/j.ejpb.2020.09.003

[10] Feczkó T., Tóth J., Dósa Gy., Gyenis J.: Optimization of protein encapsulation in PLGA nanoparticles. Chemical Engineering and Processing: Process Intensification, **50**, 757–765 (2011). https://doi.org/10.1016/j.cep.2011.06.008

[11] Silva A. L., Rosalia R. A., Sazak A., Carstens M. G., Ossendorp F., Oostendorp J., Jiskoot W.: Optimization of encapsulation of a synthetic long peptide in PLGA nanoparticles: Low-burst release is crucial for efficient $CD8^+$ T cell activation. European Journal of Pharmaceutics and Biopharmaceutics, **83**, 338–345 (2013). https://doi.org/10.1016/j.ejpb.2012.11.006

[12] Ramazani F., Chen W., van Nostrum C. F., Storm G., Kiessling F., Lammers T., Hennink W. E., Kok R. J.: Strategies for encapsulation of small hydrophilic and amphiphilic drugs in PLGA microspheres: State-of-the-art and challenges. International Journal of Pharmaceutics, **499**, 358–367 (2016). https://doi.org/10.1016/j.ijpharm.2016.01.020

[13] Rivas C. J. M., Tarhini M., Badri W., Miladi K., Greige-Gerges H., Nazari Q. A., Rodríguez S. A. G., Román R. Á., Fessi H., Elaissari A.: Nanoprecipitation process: From encapsulation to drug delivery. International Journal of Pharmaceutics, **532**, 66–81 (2017). https://doi.org/10.1016/j.ijpharm.2017.08.064

[14] Wu C., Baldursdottir S., Yang M., Mu H.: Lipid and PLGA hybrid microparticles as carriers for protein delivery. Journal of Drug Delivery Science and Technology, **43**, 65–72 (2018). https://doi.org/10.1016/j.jddst.2017.09.006

[15] Arpicco S., Battaglia L., Brusa P., Cavalli R., Chirio D., Dosio F., Gallarate M., Milla P., Peira E., Rocco F., Sapino S., Stella B., Ugazio E., Ceruti M.: Recent studies on the delivery of hydrophilic drugs in nanoparticulate systems. Journal of Drug Delivery Science and Technology, **32**, 298–312 (2016). https://doi.org/10.1016/j.jddst.2015.09.004

[16] Rietscher R., Czaplewska J. A., Majdanski T. C., Gottschaldt M., Schubert U. S., Schneider M., Lehr C-M.: Impact of PEG and PEG-*b*-PAGE modified PLGA on nanoparticle formation, protein loading and release. International Journal of Pharmaceutics, **500**, 187–195 (2016). https://doi.org/10.1016/j.ijpharm.2016.01.021

[17] Tonova K., Lazarova Z.: Reversed micelle solvents as tools of enzyme purification and enzyme-catalyzed conversion. Biotechnology Advances, **26**, 516–532 (2008). https://doi.org/10.1016/j.biotechadv.2008.06.002

[18] Dodevski I., Nucci N. V., Valentine K. G., Sidhu G. K., O'Brien E. S., Pardi A., Wand A. J.: Optimized reverse micelle surfactant system for high-resolution NMR spectroscopy of encapsulated proteins and nucleic acids dissolved in low viscosity fluids. Journal of the American Chemical Society, **136**, 3465–3474 (2014). https://doi.org/10.1021/ja410716w

[19] Fuglestad B., Marques B. S., Jorge C., Kerstetter N. E., Valentine K. G., Wand A. J.: Reverse micelle encapsulation of proteins for NMR spectroscopy. Methods in Enzymology, **615**, 43–75 (2019). https://doi.org/10.1016/bs.mie.2018.08.032

[20] Sanders A. B., Zangaro J. T., Webber N. K., Calhoun R. P., Richards E. A., Ricci S. L., Work H. M., Yang D. D., Casey K. R., Iovine J. C., Baker G., Douglas T. V., Dutko S. B., Fasano T. J., Lofland S. A., Rajan A. A., Vasile M. A., Carone B. R., Nucci N. V.: Optimization of biocompatibility for a hydrophilic biological molecule encapsulation system. Molecules, **27**, 1572 (2022). https://doi.org/10.3390/molecules27051572

[21] Derossi D.: The third helix of the antennapedia homeodomain translocates through biological membranes. Journal of Biological Chemistry, **269**, 10444–10450 (1994). https://doi.org/10.1016/S0021-9258(17)34080-2

[22] Langel Ü., Pooga M., Kairane C., Zilmer M., Bartfai T.: A galanin-mastoparan chimeric peptide activates the Na^+,K^+-ATPase and reverses its inhibition by ouabain. Regulatory Peptides, **62**, 47–52 (1996). https://doi.org/10.1016/0167-0115(96)00002-X

[23] Wada A., Wong P-F., Hojo H., Hasegawa M., Ichinose A., Llanes R., Kubo Y., Senba M., Ichinose Y.: Alarin but not its alternative-splicing form, GALP (galanin-like peptide) has antimicrobial activity. Biochemical and Biophysical Research Communications, **434**, 223–227 (2013). https://doi.org/10.1016/j.bbrc.2013.03.045

[24] Briolat J., Wu S. D., Mahata S. K., Gonthier B., Bagnard D., Chasserot-Golaz S., Helle K. B., Aunis D., Metz-Boutigue M. H.: New antimicrobial activity for the catecholamine release-inhibitory peptide from chromogranin A. CMLS, Cellular and Molecular Life Sciences, **62**, 377–385 (2005). https://doi.org/10.1007/s00018-004-4461-9

[25] Park C. B., Kim M. S., Kim S. C.: A novel antimicrobial peptide from *Bufo bufo gargarizans*. Biochemical and Biophysical Research Communications, **218**, 408–413 (1996). https://doi.org/10.1006/bbrc.1996.0071

[26] Kiss É., Gyulai G., Pári E., Horváti K., Bősze Sz.: Membrane affinity and fluorescent labelling: Comparative study of monolayer interaction, cellular uptake and cytotoxicity profile of carboxyfluorescein-conjugated cationic peptides. Amino Acids, **50**, 1557–1571 (2018). https://doi.org/10.1007/s00726-018-2630-7

[27] Horváti K., Fodor K., Pályi B., Henczkó J., Balka G., Gyulai G., Kiss É., Biri-Kovács B., Senoner Z., Bősze Sz.: Novel assay platform to evaluate intracellular killing of *Mycobacterium tuberculosis: In vitro* and *in vivo* validation. Frontiers in Immunology, **12**, 750496 (2021). https://doi.org/10.3389/fimmu.2021.750496

[28] Gasteiger E., Hoogland C., Gattiker A., Duvaud S., Wilkins M. R., Appel R. D., Bairoch A.: Protein identification and analysis tools on the ExPASy server. in 'The proteomics protocols handbook' (ed.: Walker J. M.) Humana Press, Totowa, 571–607 (2005). https://doi.org/10.1385/1-59259-890-0:571

[29] Eisenberg D.: Three-dimensional structure of membrane and surface proteins. Annual Revew of Biochemistry, **53**, 595–623 (1984). https://doi.org/10.1146/annurev.bi.53.070184.003115

[30] Dash S., Murthy P. N., Nath L., Chowdhury P.: Kinetic modeling on drug release from controlled drug delivery systems. Acta Poloniae Pharmaceutica, **67**, 217–223 (2010).

[31] Korsmeyer R. W., Gurny R., Doelker E., Buri P., Peppas N. A.: Mechanisms of solute release from porous hydrophilic polymers. International Journal of Pharmaceutics, **15**, 25–35 (1983). https://doi.org/10.1016/0378-5173(83)90064-9

[32] Peppas N. A., Sahlin J. J.: A simple equation for the description of solute release. III. Coupling of diffusion and relaxation. International Journal of Pharmaceutics, **57**, 169–172 (1989). https://doi.org/10.1016/0378-5173(89)90306-2

[33] Ziegler-Heitbroc H. W. L., Thiel E., Futterer A., Herzog V., Wirtz A., Riethmüller G.: Establishment of a human cell line (Mono Mac 6) with characteristics of mature monocytes. International Journal of Cancer, **41**, 456–461 (1988). https://doi.org/10.1002/ijc.2910410324

[34] Quentmeier H., Pommerenke C., Dirks W. G., Eberth S., Koeppel M., Roderick A. F., MacLeod R. A. F., Nagel S., Steube K., Uphoff C. C., Drexler H. G.: The LL-100 panel: 100 cell lines for blood cancer studies. Scientific Reports, **9**, 8218 (2019). https://doi.org/10.1038/s41598-019-44491-x

[35] Rampersad S. N.: Multiple applications of alamar blue as an indicator of metabolic function and cellular health in cell viability bioassays. Sensors, **12**, 12347–12360 (2012). https://doi.org/10.3390/s120912347

[36] Bordes C., Fréville V., Ruffin E., Marote P., Gauvrit J. Y., Briançon S., Lantéri P.: Determination of poly(ε-caprolactone) solubility parameters: Application to solvent substitution in a microencapsulation process. International Journal of Pharmaceutics, **383**, 236–243 (2010). https://doi.org/10.1016/j.ijpharm.2009.09.023

[37] United States Pharmacopeial Convention: Residual solvents. Interim Revision Announcement, Vol. **467**, 1–23 (2020).

[38] Derman S.: Caffeic acid phenethyl ester loaded PLGA nanoparticles: Effect of various process paraymeters on reaction yield, encapsulation efficiency, and particle size. Journal of Nanomaterials, **2015**, 341848 (2015). https://doi.org/10.1155/2015/341848

[39] Kamtsikakis A., Kavetsou E., Chronaki K., Kiosidou E., Pavlatou E., Karana A., Papaspyrides C., Detsi A., Karantonis A., Vouyiouka S.: Encapsulation of antifouling organic biocides in poly(lactic acid) nanoparticles. Bioengineering, **4**, 81 (2017). https://doi.org/10.3390/bioengineering4040081

[40] Tóth T., Kiss É.: A method for the prediction of drug content of poly(lactic-*co*-glycolic)acid drug carrier nanoparticles obtained by nanoprecipitation. Journal of Drug Delivery Science and Technology, **50**, 42–47 (2019). https://doi.org/10.1016/j.jddst.2019.01.010

[41] Ábrahám Á., Gyulai G., Tóth T., Szvoboda B., Mihály J., Szabó Á., Kiss É.: Improvement of the drug encapsulation into biodegradable polyester nanocarriers by blending of poly(lactic-*co*-glycolic acid) and polycaprolactone. Express Polymers Letters, **16**, 960–977 (2022). https://doi.org/10.3144/expresspolymlett.2022.70

[42] Ábrahám Á., Massignan F., Gyulai G., Katona M., Taricska N., Kiss É.: Comparative study of the solid-liquid interfacial adsorption of proteins in their native and amyloid forms. International Journal of Molecular Science, **23**, 13219 (2022). https://doi.org/10.3390/ijms232113219

[43] Marques B. S., Nucci N. V., Dodevski I., Wang K. W. C., Athanasoula E. A., Jorge C., Wand A. J.: Measurement and control of pH in the aqueous interior of reverse micelles. The Journal of Physical Chemistry B, **118**, 2020–2031 (2014). https://doi.org/10.1021/jp4103349

[44] Mulheran P., Kubiak K.: Protein adsorption mechanisms on solid surfaces: Lysozyme-on-mica. Molecular Simulation, **35**, 561–566 (2009). https://doi.org/10.1080/08927020802610288

[45] Komorek P., Martin E., Jachimska B.: Adsorption and conformation behavior of lysozyme on a gold surface determined by QCM-D, MP-SPR, and FTIR. International Journal of Molecular Science, **22**, 1322 (2021). https://doi.org/10.3390/ijms22031322

[46] da Rocha L., Baptista A. M., Campos S. R. R.: Approach to study pH-dependent protein association using constant-pH molecular dynamics: Application to the dimerization of β-lactoglobulin. Journal of Chemical Theory and Computation, **18**, 1982–2001 (2022). https://doi.org/10.1021/acs.jctc.1c01187

[47] Jachimska B., Świątek S., Loch J. I., Lewiński K., Luxbacher T.: Adsorption effectiveness of β-lactoglobulin onto gold surface determined by quartz crystal microbalance. Bioelectrochemistry, **121**, 95–104 (2018). https://doi.org/10.1016/j.bioelechem.2018.01.010

[48] Lošdorfer Božič A. B., Podgornik R.: pH dependence of charge multipole moments in proteins. Biophysical Journal, **113**, 1454–1465 (2017). https://doi.org/10.1016/j.bpj.2017.08.017

[49] Chung W. K., Evans S. T., Freed A. S., Keba J. J., Baer Z. C., Rege K., Cramer S. M.: Utilization of lysozyme charge ladders to examine the effects of protein surface charge distribution on binding affinity in ion exchange systems. Langmuir, **26**, 759–768 (2010). https://doi.org/10.1021/la902135t

[50] Majhi P. R., Ganta R. R., Vanam R. P., Seyrek E., Giger K., Dubin P. L.: Electrostatically driven protein aggregation: β-lactoglobulin at low ionic strength. Langmuir, **22**, 9150–9159 (2006). https://doi.org/10.1021/la053528w

[51] Trojer M. A., Nordstierna L., Nordin M., Nydén M., Holmberg K.: Encapsulation of actives for sustained release. Physical Chemistry Chemical Physics, **15**, 17727 (2013). https://doi.org/10.1039/c3cp52686k

[52] Nordstierna L., Abdalla A. A., Nordin M., Nydén M.: Comparison of release behaviour from microcapsules and microspheres. Progress in Organic Coatings, **69**, 49–51 (2010). https://doi.org/10.1016/j.porgcoat.2010.05.003

[53] Horváti K., Bacsa B., Mlinkó T., Szabó N., Hudecz F., Zsila F., Bősze Sz.: Comparative analysis of internalisation, haemolytic, cytotoxic and antibacterial effect of membrane-active cationic peptides: Aspects of experimental setup. Amino Acids, **49**, 1053–1067 (2017). https://doi.org/10.1007/s00726-017-2402-9